1758 Vol. 36, No. 7 / July 2019 / Journal of the Optical Society of America B Research Article

Journal of the Optical Society of America B OPTICAL PHYSICS

Electromagnetically induced transparency with a single frequency comb mode probe

I. Krešić,[1,2,*] M. Kruljac,[1] T. Ban,[1] and D. Aumiler[1]

[1]Institute of Physics, Bijenička c. 46, 10000 Zagreb, Croatia
[2]Institute of Theoretical Physics, Vienna University of Technology, Vienna A-1040, Austria
*Corresponding author: ikresic@ifs.hr

Received 26 February 2019; revised 8 May 2019; accepted 16 May 2019; posted 16 May 2019 (Doc. ID 361122); published 11 June 2019

We measure the electromagnetically induced transparency (EIT) of a single-frequency comb mode interacting with laser-cooled ^{87}Rb atoms. A Λ hyperfine level structure in a D2 transition is used in the configuration of co-propagated probe (frequency comb) and coupling (continuous-wave) laser fields. The signature of EIT in the transmission of a single comb mode as well as the radiation pressure force is experimentally detected. The results are satisfactorily reproduced by the developed theoretical models, where EIT is seen to occur due to coherent accumulation. Our results could find application in quantum computing and communication with optical frequency combs.

https://doi.org/10.1364/JOSAB.36.001758

1. INTRODUCTION

Electromagnetically induced transparency (EIT) is a phenomenon wherein the elimination of absorption at resonance occurs due to destructive interference of transition amplitudes belonging to different excitation pathways [1]. The applications of EIT range from efficient generation of coherent radiation in new frequency domains [2] to the generation of slow light [3] for the realization of quantum memories [4], potentially used in quantum communication and computing [5].

Optical frequency combs (FCs) are unique sources of light. In the time domain they are represented by a train of phase-stabilized ultrashort pulses, while in the frequency domain their spectrum consists of a large number of equidistant narrow lines whose frequency can be stabilized and determined with high accuracy. Due to their pulsed nature, FCs provide high peak powers needed for efficient frequency conversion while simultaneously preserving long coherence times. FCs have revolutionized high-resolution spectroscopy [6–8] and frequency metrology [9,10]. Furthermore, the recent progress in generating highly multimode nonclassical FCs in femtosecond (fs) synchronously pumped optical parametric oscillators [11–16], or by spontaneous four-wave mixing in microring resonators [17,18], extends their significance to the fields of quantum computing and communication. Temporal multimode quantum memories based on the atomic FCs were considered in [19,20]. More recently an interesting proposal was made toward realizing quantum memories for photons in a large number of frequency modes (i.e., frequency multimode) contained in a nonclassical optical FC, which could increase the capacity of quantum information storage [21]. As this type of quantum memory is yet to be experimentally realized, we here aim to explore one of the building blocks of the proposal, the transfer of coherence from an ultrashort pulse FC to the atomic ground states in a Λ level structure.

Quantum interference in an atomic three-level Λ system excited by an ultrashort fs pulse train, i.e., a FC in the frequency domain, has been investigated theoretically in [22,23]. It was shown that, in the condition when the pulse repetition period is shorter than the characteristic atomic relaxation times and the pulse repetition rate is a subharmonic of the two lowest energy states, coherent accumulation of excitation leads to the phenomena of EIT and coherent population trapping. Experimental demonstrations of EIT with frequency combs include the EIT in rubidium vapor prepared by a mode-locked diode laser frequency comb [24], mode-locked rubidium laser [25], and potassium vapor probed by an electro-optic frequency comb [26]. However, no demonstration of EIT with optical FCs producing pulses as short as ∼100 fs was reported in the literature thus far, to the best of our knowledge.

In this paper we report the observation of single fs FC mode EIT in cold ^{87}Rb atoms. A Λ configuration of hyperfine levels in the $|5S_{1/2}\rangle \rightarrow |5P_{3/2}\rangle$ D2 transition is used with a coupling field obtained from a cw laser. The EIT is experimentally demonstrated by measuring the transmission of a single comb line using heterodyne spectroscopy and by measuring the radiation pressure force of the cloud due to interaction with the probe (FC) and coupling (cw) laser fields. Theoretical models based on optical Bloch equations (OBEs) are developed and applied in the interpretation of experimental results. The FC EIT is seen to be a result of coherent accumulation of excitation by a train of ultrashort pulses, transferred to the atomic ground

states via the coupling laser. The experimental findings are reproduced by the theory to a satisfactory degree. We note that our setup involves a single FC mode probe and a cw coupling beam interacting with the atomic hyperfine levels, and the observed effect should not be confused with the coherent phenomena observed with a single laser beam, e.g., in magneto-optics [27].

2. EXPERIMENTAL SETUP

A cold rubidium cloud is loaded from background vapor in a stainless steel chamber. The magneto-optical trap (MOT) is realized by intersecting six cw laser beams, which, together with an anti-Helmholtz produced quadrupole magnetic field and a repumper laser, create the trapping geometry. Fluorescence imaging of the cloud is performed with a camera aligned along an axis in the horizontal plane. In typical experimental conditions we obtain a cloud 1.6 mm in diameter, which contains $\sim 10^8$ atoms at a temperature of about 150 μK. This cold cloud represents the optical medium for our EIT measurements.

We study EIT in a Λ-type configuration with the co-propagated coupling (cw) and probe (FC) laser beams; see Figs. 1(a) and 1(b). The coupling beam is obtained from a diode laser (Toptica DL 100) with nominal emission at 780 nm, output power of about 40 mW, and a linewidth of about 1 MHz. It is stabilized to a $F = 1 \rightarrow F' = 1$ transition in ^{87}Rb using saturation spectroscopy. In order to obtain the $F = 1 \rightarrow F' = 2$ frequency needed for the EIT measurements, as well as to control its detuning and power, a laser is sent through an acousto-optic modulator (AOM) in a double-pass configuration. The probe beam is the nth line of a FC generated by frequency doubling an Er:fiber mode-locked laser (TOPTICA FFS) operating with a repetition rate $f_{\text{rep}} = 80.54$ MHz, an output power of $P \approx 230$ mW, and a FWHM ≈130 nm spectrum centered around 1560 nm. The frequency-doubled spectrum used in the experiment is centered around 780 nm with a FWHM bandwidth of about 5 nm and a total power of 76 mW. Approximately 90,000 comb lines are contained under the FC spectral envelope. The FC is stabilized to a cw reference laser (ECDL, Moglabs CEL002) locked to the $^{87}\text{Rb}|5S_{1/2}; F = 2\rangle \rightarrow |5P_{3/2}; F' = 3\rangle$ transition, while the pulse train repetition frequency is locked to a stable microwave reference [28]. The frequency of the comb modes can be continuously scanned within one f_{rep} range by changing the beat frequency used for stabilization of the FC to the optical reference. The two beams (cw and FC) have similar FWHM of 1.3 and 1.9 mm, respectively, mutually orthogonal polarizations, and co-propagate in the $x - y$ plane and at an angle of 45° to one of the trapping beams.

EIT is demonstrated by measuring the radiative force on the cold cloud due to the interaction with both probe (FC) and coupling (cw) laser fields and by measuring the transmission of a single comb line.

Measurement of the radiative force. Both EIT beams (FC and cw) are carefully overlapped and directed to the center of the MOT where the cold cloud of Rb atoms is prepared. The measurement sequence starts with the preparation of a cold ^{87}Rb cloud and both EIT beams off. At $t = 0$ we turn off

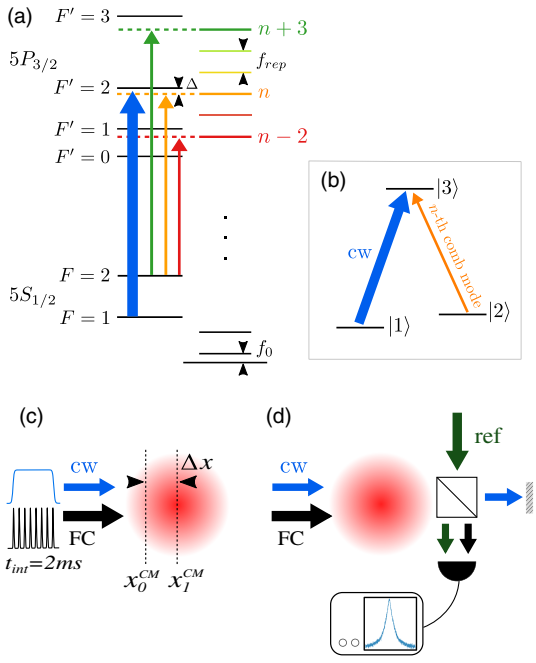

Fig. 1. Scheme for observing the single FC mode EIT. (a) Energy levels of the ^{87}Rb D2-line. A cw coupling laser is resonant with the $F = 1 \rightarrow F' = 2$ transition, and the nth FC mode detuning Δ is scanned over the $F = 2 \rightarrow F' = 2$ transition. The nth comb mode has here the role of a probe. The other transitions, driven by the $(n + 3)$rd and $(n - 2)$nd comb modes, do not contribute significantly to EIT and can be neglected, producing (b) an effective Λ-system. (c) Setup schematics for the radiative force measurements. Radiative force on cold rubidium atoms induced by co-propagated cw (blue) and FC (black) laser beams is determined by measuring the cloud center of mass displacement in the beam propagation direction. (d) Schematics for measuring the transmission of a single comb mode. After passing through the cloud, the cw coupling beam is separated from the FC beam on a polarizing beam splitter (PBS) and blocked from further measurements. Using a PBS the FC beam is co-propagated with a reference (green) cw laser beam stabilized close to the $F = 2 \rightarrow F' = 2$ transition and a beat with the nth FC mode is observed on a spectrum analyzer.

the MOT beams (cooling and repumper), and switch on the EIT beams. We let the EIT beams interact with the cold cloud for 2 ms. During this time the cloud center of mass (CM) accelerates along the EIT beam propagation axis (+x-direction) due to the radiation pressure force. At $t = 2$ ms, both beams are switched off, and the cloud moves freely for 1.5 ms after which the MOT beams are turned on for 0.2 ms and the cloud fluorescence is imaged with a camera to determine the cloud's center of mass displacement in the x direction, Δx; see Fig. 1(c). The free expansion time of 1.5 ms is chosen to optimize both the accuracy of the CM measurement and the signal-to-noise ratio. We then use Δx to calculate the acceleration of the cloud, which, using the Rb atom mass, finally gives the total force due to the FC and the cw laser.

Measurement of single comb mode transmission. In these measurements the FC beam is focused onto the center of the MOT to a FWHM of ≈0.60 mm, and the cw beam is directed

to the MOT center with the same diameter as previously. After traversing the cloud, the cw coupling beam is separated from the FC beam on a polarizing beam splitter (PBS) and blocked from further measurements; see Fig. 1(d). On the same PBS, the FC beam is overlapped with an additional cw reference beam derived from the cooling laser (ECDL Moglabs CEL002) and tuned near the $F = 2 \rightarrow F' = 2$ transition by an AOM, with its power kept constant during scans. The beat note between the cw reference beam and the nth comb mode is detected by using heterodyne spectroscopy. The beat signal was detected using a photodiode (Thorlabs PDA10A-EC) with a filtering and amplification stage before readout on a spectrum analyzer (Rigol DSA1030A). The square of the area below the beat signal is proportional to the product of the reference laser and the nth comb mode intensities. The transmission of the nth comb line, $I_n/I_{n,0}$, is extracted from the measured beat signals by dividing the squared trace when the MOT beams are on (I_n), by the squared trace when the MOT beams are off ($I_{n,0}$), with the reference beam intensity kept constant during the measurements. We note that during these measurements the cooling and repumper beams were switched on, which is not expected to preclude the EIT, as was demonstrated by transmission measurements in [29].

3. THEORY OF SINGLE COMB MODE EIT

In this section we present the two models used for describing our system: a six-level model for the hyperfine D2 line of ^{87}Rb and a three-level Λ scheme. We give the numerical solutions for the six-level model, the three-level model calculated in the impulse approximation [30], and provide an analytical solution for the three-level model valid to the first order in the probe Rabi frequency. The comparison of the solutions for the six-level and the three-level models indicates that the latter is sufficient to describe the physics of single FC mode EIT in the ^{87}Rb D2 line at low single comb Rabi frequencies.

A. Six-Level Model

We now describe the equations for modeling of the atom–light interaction of the FC and cw beams with the hyperfine D2 line of ^{87}Rb. The equations for the six-level model are similar to those given in [31]. The Liouville equation for a density matrix element $\rho_{m,n} = \langle n|\rho|m\rangle$ has the form

$$\frac{d}{dt}\rho_{m,n} = -\frac{i}{\hbar}\langle n|[H,\rho]|m\rangle - \Gamma_{m,n}\rho_{m,n}, \tag{1}$$

where H is the Hamiltonian and $\Gamma_{m,n}$ is equal to $\Gamma = 2\pi \times 6.066$ MHz for excited-state populations and coherences, $\Gamma/2$ for optical coherences and zero otherwise [32]. The indices m and n go from 1 to 6 with ascending order in the corresponding state energy [see Fig. 1(a)]. The Hamiltonian has the form $H = H_0 + H_{\text{int}}$, where H_0 is the Hamiltonian of the free atom and $(H_{\text{int}})_{m,n} = -\mu_{mn}(E_T(t) + \mathcal{E}_c e^{i\omega_c t})$ (where ω_c is the frequency of the cw coupling laser). The dipole transition moments μ_{mn} are taken from [32]. The femtosecond pulse train electric field is given by $E_T(t) = E_f(t)e^{i\omega_{fs}t}$, where $E_f(t) = \sum_{n=0}^{\infty}\mathcal{E}(t - nT_R)e^{in\Phi_R}$, ω_{fs} is the center frequency of the fs field, and Φ_R is the phase acquired by the field in a round trip along the laser cavity. The spectrum of the fs laser has the structure of a comb centered around $\omega_{fs} + \Phi_R/T_R$ with lines separated by $1/T_R$, where T_R is the pulse repetition rate. In the following we use for the pulses: $\mathcal{E}(t) = \mathcal{E}_f \text{sech}(1.763t/T_p)$, where $\mathcal{E}_f$ is the peak FC electric field and T_p is the pulse duration.

Equation (1) is written and solved in the rotating wave approximation (RWA), where the populations (diagonal elements) are given by $\rho_{m,m}$ and the coherences (off-diagonal elements) are given by their slowly varying envelopes $\rho_{m,n}e^{-i\omega_{fs}}$. Additional terms were added to Eq. (1) to account for the repopulation of the ground states by spontaneous excited-state relaxation, calculated via the Clebsch–Gordan coefficients for the D2 line of ^{87}Rb given in [32]. The initial conditions for the numerical solving procedure are that the population in the state $F = 2$ is equal to 1 and is the only finite density matrix element, which corresponds to the experimental situation.

B. Three-Level Model

We now describe the Λ model, used to approximate the interaction of a single frequency comb mode and a cw pump field with the substructure of the D2 line spanned by the states $|1\rangle = |F=1\rangle, |2\rangle = |F=2\rangle$ and $|3\rangle = |F' = 2\rangle$ [see Fig. 1(b)]. We here write the Hamiltonian in the RWA as

$$H = \Delta|2\rangle\langle 2| + \Delta_c|1\rangle\langle 1| - (\mu_{23}E_f(t)\hbar|3\rangle\langle 2| + \mu_{13}\mathcal{E}_c\hbar|3\rangle\langle 1| + \text{h.c.}), \tag{2}$$

where $E_f(t)$ is the slowly varying envelope of the fs field and $\mathcal{E}_c$ is the amplitude of the cw field, with $\Delta = \omega_{fs} - \omega_{23}$, $\Delta_c = \omega_c - \omega_{13}$ [ω_{13}, ω_{23} are the frequencies of the transitions $|1\rangle \rightarrow |3\rangle$ and $|2\rangle \rightarrow |3\rangle$ in Fig. 1(b)] and μ_{13}, μ_{23} being the dipole transition moments.

As in [30], we divide the dynamics during T_R into two stages: during and after the pulse duration. During the pulse duration, the electric field $\mathcal{E}_c$ is ignored and the dynamical equations are solved analytically, giving the solutions after the nth pulse:

$$\begin{aligned}
\rho_{2,2}^{n,\tau} &= \rho_{2,2}^n \cos^2(\theta/2) + \rho_{3,3}^n \sin^2(\theta/2) + \text{Im}(\rho_{2,3}^n)\sin\theta,\\
\rho_{3,3}^{n,\tau} &= \rho_{2,2}^n \sin^2(\theta/2) + \rho_{3,3}^n \cos^2(\theta/2) - \text{Im}(\rho_{2,3}^n)\sin\theta,\\
\rho_{2,1}^{n,\tau} &= \rho_{2,1}^n \cos(\theta/2) + i\rho_{3,1}^n \sin(\theta/2),\\
\rho_{2,3}^{n,\tau} &= \frac{i}{2}(\rho_{3,3}^n - \rho_{2,2}^n)\sin\theta + \rho_{2,3}^n \cos^2(\theta/2) + \rho_{3,2}^n \sin^2(\theta/2),\\
\rho_{3,1}^{n,\tau} &= \rho_{3,1}^n \cos(\theta/2) + i\rho_{2,1}^n \sin(\theta/2),
\end{aligned} \tag{3}$$

where $\rho_{i,j}^{n,\tau}$ is the element $\langle i|\hat{\rho}|j\rangle$ of the density matrix at a time τ after the nth pulse, $\rho_{i,j}^n$ is the same element before this pulse, and $\theta = \frac{2\mu_{23}}{\hbar}\int_{-\infty}^{\infty}\mathcal{E}(t)\text{d}t$ is the pulse area. The time τ is sufficiently long that the pulse has decayed, but still $\tau \ll T_R$ so that the dynamics due to $\mathcal{E}_c$ can be neglected. In the time between $t = \tau$ and $t = T_R$, the dynamics is determined by interaction with $\mathcal{E}_c$, and the dynamical equations are now

$$\frac{d}{dt}\rho_{2,2} = \frac{\Gamma}{2}\rho_{3,3},$$
$$\frac{d}{dt}\rho_{3,3} = -\Gamma\rho_{3,3} + \Omega_c \mathrm{Im}(\rho_{3,1}),$$
$$\frac{d}{dt}\rho_{2,1} = -i\left((\Delta - \Delta_c)\rho_{2,1} + \frac{1}{2}\Omega_c\rho_{2,3}\right),$$
$$\frac{d}{dt}\rho_{2,3} = -\frac{\Gamma}{2}\rho_{2,3} - i\left(\Delta\rho_{2,3} + \frac{1}{2}\Omega_c\rho_{2,1}\right),$$
$$\frac{d}{dt}\rho_{3,1} = -\frac{\Gamma}{2}\rho_{3,1} + i\left(\Delta_c\rho_{3,1} + \frac{1}{2}\Omega_c(\rho_{1,1} - \rho_{3,3})\right), \quad (4)$$

where $\Omega_c = 2\mu_{13}\mathcal{E}_c/\hbar$ is the Rabi frequency of the cw laser and Γ is the decay rate of the excited-state population, taken as equal for both optical transitions. To calculate the steady-state behavior we iteratively solve Eq. (4) for the initial conditions of $\rho_{2,2} = 1$ with all other matrix elements equal to zero, and conditions at the nth pulse given by Eq. (3). The approach outlined here is justified as $\mathcal{E}_f \gg \mathcal{E}_c$ and T_p is orders of magnitude smaller than the quantities: $T_R, \Delta_c^{-1}, \Delta^{-1}, \Gamma^{-1}$.

We have calculated the steady-state solutions of Eqs. (3) and (4) to the first order in the single comb mode Rabi frequency. This is done by a perturbative density matrix expansion of the form $\rho_{i,j} = \rho_{i,j}^{(0)} + \rho_{i,j}^{(1)} + \rho_{i,j}^{(3)} + \cdots$. In the work of [33] the expansion was used for a small Rabi frequency probe and a large Rabi frequency coupling beam, both cw. The Rabi frequency of a single FC mode (Ω_f) is in our case indeed very low, as confirmed in the work of [28]. We can thus implement the results of [33], where to the first order in Ω_f the $\rho_{2,1}^{(1)}$, $\rho_{2,3}^{(1)}$, and the zeroth-order population $\rho_{2,2}^{(0)} = 1$ are the only finite density matrix elements. Using these results with our dynamical equations it can be shown that the first-order solutions after an nth pulse evolve as

$$\rho_{2,1}^{(1)}(t) = e^{-\frac{\Gamma}{4}t - i\Delta t}\left(\rho_{2,1}^{n}\cos(\theta/2)f_+(t) - \left(\frac{1}{2}\sin\theta + i\rho_{2,3}^{n}\cos^2(\theta/2) + i\rho_{3,2}^{n}\sin^2(\theta/2)\right)g(t)\right),$$
$$\rho_{2,3}^{(1)}(t) = e^{-\frac{\Gamma}{4}t - i\Delta t}\left(-i\rho_{2,1}^{n}\cos(\theta/2)g(t) - \left(\frac{i}{2}\sin\theta - \rho_{2,3}^{n}\cos^2(\theta/2) - \rho_{3,2}^{n}\sin^2(\theta/2)\right)f_-(t)\right), \quad (5)$$

with all the other matrix elements equal to zero, the function $f_\pm(t)$ given by

$$f_\pm(t) = \begin{cases} \cosh(\eta t/2) \pm \frac{\Gamma}{2\eta}\sinh(\eta t/2), & \Omega_c < \frac{\Gamma}{2} \\ 1 \pm \frac{\Gamma}{4}t, & \Omega_c = \frac{\Gamma}{2}, \\ \cos(\eta t/2) \pm \frac{\Gamma}{2\eta}\sin(\eta t/2), & \Omega_c > \frac{\Gamma}{2} \end{cases} \quad (6)$$

and the function $g(t)$ given by

$$g(t) = \begin{cases} \frac{\Omega_c}{\eta}\sinh(\eta t/2), & \Omega_c < \frac{\Gamma}{2} \\ \frac{\Gamma}{4}t, & \Omega_c = \frac{\Gamma}{2}, \\ \frac{\Omega_c}{\eta}\sin(\eta t/2), & \Omega_c > \frac{\Gamma}{2} \end{cases} \quad (7)$$

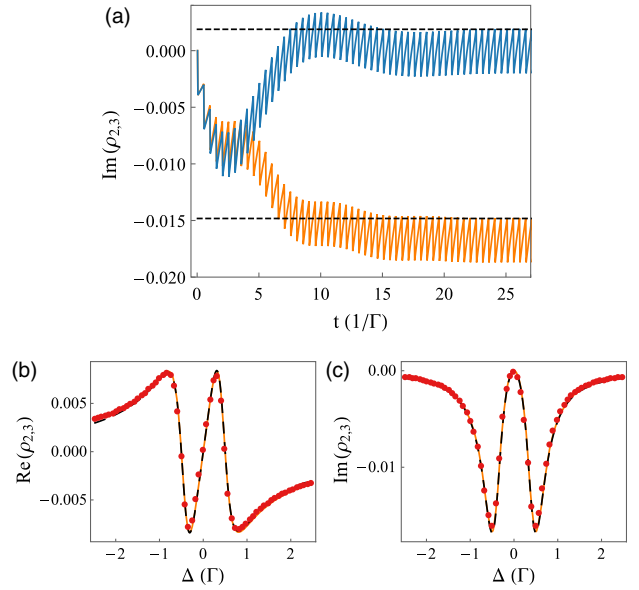

Fig. 2. Theoretical prediction of single comb mode EIT. (a) Time dependence of the imaginary part of optical coherence $\rho_{2,3}$ in a Λ model. The orange and blue curves show the numerical solutions of Eqs. (3) and (4) at $\Delta = 0.5\Gamma$ and $\Delta = 0$, respectively. The dashed horizontal lines are the analytical steady-state first-order solutions (see text), proportional to the negative absorption coefficient [1]. Steady-state (b) real and (c) imaginary parts of the optical coherence excited by the nth comb mode. The solid orange lines are the numerical solutions in the Λ model via the impulse approximation [30]. The dashed black lines are steady-state analytical calculations in the first order (see text). The red dots are calculated numerically from the six-level model. Parameters: $\mathcal{E}_c = 86.96$ V/m, $\mathcal{E}_f = 5.03 \times 10^4$ V/m, $\Delta_c = 0$, 150 pulses, $T_p = 200$ fs, $1/T_{\mathrm{rep}} = 80.54$ MHz.

where $\eta = \sqrt{|\Omega_c^2 - \Gamma^2/4|}$ and for simplicity we have put $\Delta_c = 0$. The solutions Eq. (5) describe transfer of coherence from the FC driven optical coherence to the ground-state coherence, enabled by a finite Ω_c. Using these solutions, we can analytically calculate the first-order steady-state solutions. The steady-state condition is fulfilled when the solutions $\rho_{2,1}^{(1)}(T_R)$ and $\rho_{2,3}^{(1)}(T_R)$ are equal to $\rho_{2,1}^{n}$ and $\rho_{2,3}^{n}$, respectively [30].

At small θ values, the first-order solution is expected to correspond to the full solution of Eqs. (3) and (4). Figure 2(a) shows the time evolution of the imaginary part of $\rho_{2,3}$ at $\Delta = 0$ and $\Delta = 0.5\Gamma$. The short-term dynamics is determined by FC pulse kicks, in between which the cw beam drives the $|1\rangle \rightarrow |3\rangle$ transition. For both detunings, the $\mathrm{Im}(\rho_{2,3})$ initially increases due to the FC kicks; however, the slower scale evolution drives the atoms in absorbing and nonabsorbing steady states for finite and zero Δ, respectively. The dashed horizontal line marks the analytically calculated steady-state solution Eq. (5). The excellent agreement of these predictions with the two solid curves is a demonstration that in our parameter regime the first-order optical coherence is indeed the dominant term of the perturbative expansion.

This is confirmed in Figs. 2(b) and 2(c) where Δ scans of steady-state real and imaginary optical coherences $\rho_{2,3}$ are shown. The numerical steady-state values are calculated by

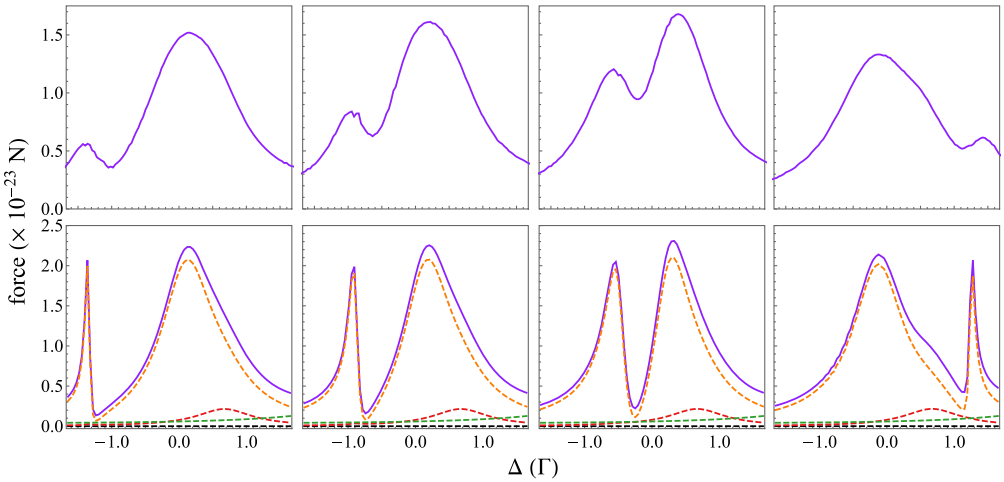

Fig. 3. Experimental (top row) and numerical (bottom row) scans of the radiation pressure force against FC detuning Δ, for varying Δ_c. Purple solid line: total force. Orange dashed line: force due to excitation of $F' = 2$. Red dashed line: force due to excitation of $F' = 1$. Green dashed line: force due to excitation of $F' = 3$. Black dashed line: force due to excitation of $F' = 0$. Columns: scans for different coupling beam detunings Δ_c of (from left to right) -1.2Γ, -0.7Γ, -0.3Γ, and 1.2Γ. The experimentally used powers of 0.3 and 15 mW for the coupling and the FC beams correspond to the numerically used electric fields $\mathcal{E}_c = 70$ V/m and $\mathcal{E}_f = 5 \times 10^4$ V/m to within the measurement uncertainty.

averaging over the last five pulses. To compare the analytical values to the numerical ones, a half an FC kick is given to the steady-state solution, calculated from the fourth equation in Eq. (3) as $\mathrm{Re}(\rho_{2,3}^{(1)}) \to \mathrm{Re}(\rho_{2,3}^{(1)})$ and $\mathrm{Im}(\rho_{2,3}^{(1)}) \to \mathrm{Im}(\rho_{2,3}^{(1)})$ $\cos\theta - \frac{\sin\theta}{4}$. This prescription is valid as the numerical steady-state value averaged over the last N pulses is approximately equal to the arithmetic mean of the maximal and minimal coherence values, which is exactly the analytical steady state with a half an FC kick [see Fig. 2(a)]. The real part of the coherence features regions of anomalous dispersion, along with a normal dispersion around the resonance, a signature of EIT [1]. The imaginary part of the coherence exhibits a characteristic EIT feature at resonance, as expected. The agreement between the full six-level numerical solution and the numerical and analytical first-order solutions of Eqs. (3) and (4), is excellent. This leads to two conclusions: (i) that the interaction of a single comb mode tuned near the $F = 2 \to F' = 2$ transition and the coupling (cw) laser tuned near the $F = 1 \to F' = 2$ transition with the atoms can be modeled by the Λ model, and (ii) that the calculated $\mathrm{Im}(\rho_{2,3})$ and $\mathrm{Re}(\rho_{2,3})$ are proportional to linear absorption and refraction of the single FC comb mode.

4. OBSERVING SINGLE COMB MODE EIT

To experimentally test single comb mode EIT in a cold ^{87}Rb sample, we first measure the radiative force on a cloud released from a MOT and irradiated by co-propagating FC and cw beams [see Fig. 1(c)]. The FC frequency scans for different coupling beam detunings Δ_c are shown in Fig. 3. For a detuned cw beam the scan exhibits dips at positions where $\Delta_c = \Delta$, a signature of two-photon Raman transitions [1]. As only a single FC satisfies the Raman condition for a given comb center frequency, this is an indirect demonstration of two-photon Raman transitions of a cw and a single FC mode. In somewhat related work, comb driven Raman transitions were experimentally utilized in trapped ions with picosecond laser pulses to entangle hyperfine clock states [34].

To disentangle the contributions of different transitions, driven by the near-detuned comb modes, on the measured radiative force, we have performed numerical simulations for 1000 pulses using the six-level system. In the steady state, the force from each transition is proportional to the population in the corresponding excited state [35,36]. In Fig. 3 we plot the force calculated for the experimental parameters from the excited-state populations, by using the Ehrenfest theorem [35]. The dominant contribution to the driving stems from the nth comb mode and the coupling beam exciting the $F' = 2$ level; however, there is also a contribution of the $(n-2)$nd mode driving the $F = 2 \to F' = 1$ transition, as witnessed by a significant population in the state $F' = 1$. For larger positive Δs, there is also a weak contribution from the $F = 2 \to F' = 3$ transition, driven by the $(n+3)$rd mode. For all detunings the peaks in the total excited-state population are asymmetric due to the $(n-2)$nd comb mode driving, and the dips do not reach zero. The main features of the theoretical curves are reproduced well in the experimental results, although it is seen that the peak asymmetry is greater in experiment, and the EIT dips are shallower and broader.

The scans at fixed $\Delta_c = 0$ for different coupling beam powers are shown in Fig. 4. The scans have the characteristic form of a Lorentzian with an EIT dip of subnatural width (for small $\mathcal{E}_c$) at $\Delta = 0$. The dips in both the experimental and theoretical plots become wider with coupling beam power as a consequence of an increase in Autler–Townes splitting [1]. The experimental plots again show shallower dips than the simulations. The discrepancies between experimental and numerical curves seen in Figs. 3 and 4 are reasonable considering that the numerical calculations do not account for all physical parameters of the experiment, e.g., Zeeman splitting due to the gradient magnetic field [37], finite laser linewidths [29],

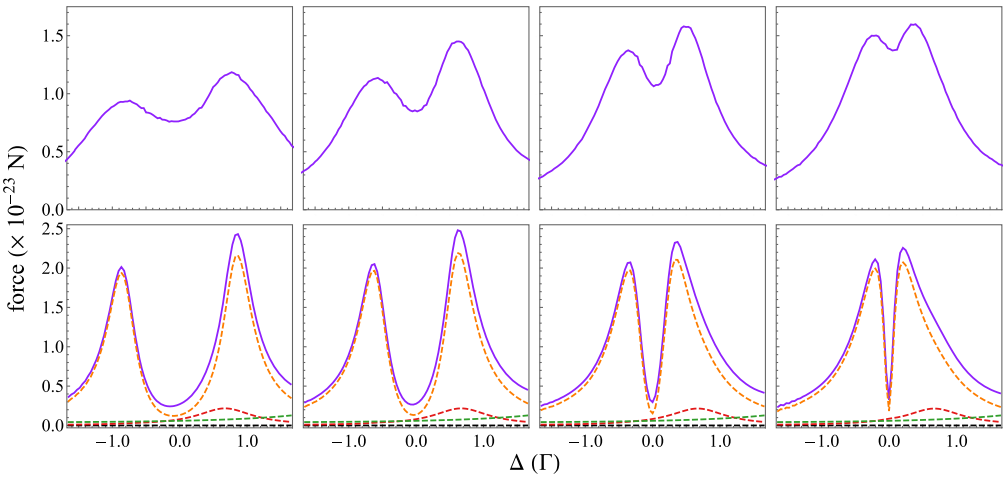

Fig. 4. Experimental (top row) and numerical (bottom row) scans of the radiation pressure force against FC detuning Δ, for varying coupling beam powers at $\Delta_c = 0$. The figure layout is the same as in Fig. 3, except that the upper columns now correspond to different coupling beam powers of (from left to right) 1.55 mW, 0.8 mW, 0.25 mW, and 80 μW and the lower columns correspond to different $\mathcal{E}_c$ fields of (from left to right) 150 V/m, 110 V/m, 60 V/m, and 35 V/m.

random dephasing of the probe and coupling beams, variation of beam intensity along the cloud, and atomic motion effects.

In experiments with two cw lasers EIT is usually observed by directly measuring the transmission of a weak probe beam after interacting with the optical medium. As the FC spectrum consists of tens of thousands of comb lines, the variation of intensity of a single comb line contributes negligibly to the variation of the total FC intensity. Therefore, it was not possible to use a typical transmission measurement setup. To observe the absorption of a single comb mode we thus use a novel technique based on measuring a heterodyne beat note of the FC and an independent cw reference beam tuned near the $F = 2 \rightarrow F' = 2$ transition, as outlined in Section 2. The results of the measurements at FC power of 15 mW and the coupling beam turned off and on (to a power of 0.6 mW) are shown in Fig. 5. When the coupling beam is turned off (blue squares), a clear transmission dip is observed. When the coupling beam is turned on with $\Delta_c \approx 0.16\Gamma$ (red circles), an increase in transmission is seen near resonance. The transmission is nearly 5 times larger than in the case with the coupling beam off. A complete transparency is not observed in this case due to the same reasons as stated above, and there is a slight asymmetry in the left and right peak heights, which can be attributed to the small blue detuning of the coupling beam. The results of Fig. 5 represent both the first reported measurements of single comb mode transmission and single comb mode EIT, to the best of our knowledge.

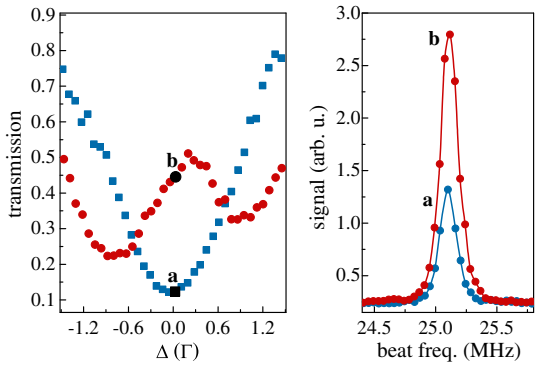

Fig. 5. Left: experimental scans of nth comb mode transmission against detuning Δ from the $F = 2 \rightarrow F' = 2$ transition. The blue squares (red circles) correspond to a scan with the coupling laser off (on). The beat signals for the data points marked (a) and (b) are shown in the plot on the right (lines are guides to the eye). To get the data points in the left plot the beat signal is squared and the area under the curve summed. This quantity is then divided by the same quantity for the case when the MOT was turned off.

5. CONCLUSION

In conclusion, we have demonstrated the EIT of a single fs frequency comb mode in a Λ-type system in a cold ^{87}Rb atom medium with a (cw) coupling laser. EIT of a single comb mode is demonstrated by measuring its transmission using heterodyne spectroscopy. In such a way it was possible to isolate a single comb mode out of the remaining tens of thousands, and to measure the small variations in its intensity within the large background stemming from the other comb modes. To the best of our knowledge, this is the first time such a technique is used for the measurement of single comb transmission. In addition to these direct EIT measurements, we have observed the EIT signature in the radiative force induced on the atomic cloud due to the interaction with both FC and cw beams.

A theoretical model based on OBEs describing the interaction of the six-level atom with the two laser fields (FC and cw) is developed and applied for the interpretation of experimental results. The experimental findings are well reproduced by theory, and they are qualitatively similar to the observations of EIT in cold rubidium atoms by using standard schemes based on two cw laser beams [29]. The six-level model was compared to a simplified three-level model in which all atomic levels other than the Λ substructure are neglected. The excellent agreement of the steady-state absorption and refraction in

the six-level model with the analytically calculated three-level results are proof that the additional comb modes do not introduce dephasing, allowing for single comb mode addressing in a real system.

Our work represents a step toward the realization of a multimode quantum memory based on EIT and Raman transitions in atomic or molecular systems excited by multimode frequency combs. We believe that in the future experiments the cw coupling laser can readily be replaced by an additional high-power FC, thus offering a series of multiple pairs of probe and coupling laser fields. An extension of the setup into the domain of nonclassical FCs would then enable storage and readout of multimode photonic quantum states, which would constitute a major advancement in quantum information processing and communication [21].

Funding. OeAD-GmbH (OEAD); Hrvatska Zaklada za Znanost (HRZZ) (IP-2014-09-7342).

Acknowledgment. I. K. gratefully acknowledges a Postdoctoral Fellowship from the Scholarship Foundation of the Republic of Austria.

REFERENCES

1. M. Fleischhauer, A. Imamoglu, and J. P. Marangos, "Electromagnetically induced transparency: Optics in coherent media," Rev. Mod. Phys. **77**, 633–673 (2005).
2. J. Harris, S. E. Field, and A. Imamoğlu, "Nonlinear optical processes using electromagnetically induced transparency," Phys. Rev. Lett. **64**, 1107–1110 (1990).
3. L. V. Hau, S. E. Harris, Z. Dutton, and C. H. Behroozi, "Light speed reduction to 17 metres per second in an ultracold atomic gas," Nature **397**, 594–598 (1999).
4. D. F. Phillips, A. Fleischhauer, A. Mair, R. L. Walsworth, and M. D. Lukin, "Storage of light in atomic vapor," Phys. Rev. Lett. **86**, 783–786 (2001).
5. L. Ma, O. Slattery, and X. Tang, "Optical quantum memory based on electromagnetically induced transparency," J. Opt. **19**, 043001 (2017).
6. A. Marian, M. C. Stowe, J. R. Lawall, D. Felinto, and J. Ye, "United time-frequency spectroscopy for dynamics and global structure," Science **306**, 2063–2068 (2004).
7. F. Adler, M. J. Thorpe, K. C. Cossel, and J. Ye, "Cavity-enhanced direct frequency comb spectroscopy: Technology and applications," Annu. Rev. Anal. Chem. **3**, 175–205 (2010).
8. B. Lomsadze and S. T. Cundiff, "Frequency combs enable rapid and high-resolution multidimensional coherent spectroscopy," Science **357**, 1389–1391 (2017).
9. T. Udem, R. Holzwarth, and T. W. Hänsch, "Optical frequency metrology," Nature **416**, 233–237 (2002).
10. A. D. Ludlow, M. M. Boyd, J. Ye, E. Peik, and P. O. Schmidt, "Optical atomic clocks," Rev. Mod. Phys. **87**, 637–701 (2015).
11. G. J. De Valcarcel, G. Patera, N. Treps, and C. Fabre, "Multimode squeezing of frequency combs," Phys. Rev. A **74**, 061801 (2006).
12. O. Pinel, P. Jian, R. M. De Araujo, J. Feng, B. Chalopin, C. Fabre, and N. Treps, "Generation and characterization of multimode quantum frequency combs," Phys. Rev. Lett. **108**, 083601 (2012).
13. J. Roslund, R. M. De Araujo, S. Jiang, C. Fabre, and N. Treps, "Wavelength-multiplexed quantum networks with ultrafast frequency combs," Nat. Photonics **8**, 109–112 (2014).
14. M. Chen, N. C. Menicucci, and O. Pfister, "Experimental realization of multipartite entanglement of 60 modes of a quantum optical frequency comb," Phys. Rev. Lett. **112**, 120505 (2014).
15. Y. Cai, J. Roslund, G. Ferrini, F. Arzani, X. Xu, C. Fabre, and N. Treps, "Multimode entanglement in reconfigurable graph states using optical frequency combs," Nat. Commun. **8**, 15645 (2017).
16. S. K. Lee, N. S. Han, T. H. Yoon, and M. Cho, "Frequency comb single-photon interferometry," Commun. Phys. **1**, 51 (2018).
17. C. Reimer, M. Kues, P. Roztocki, B. Wetzel, F. Grazioso, B. E. Little, S. T. Chu, T. Johnston, Y. Bromberg, L. Caspani, D. J. Moss, and R. Morandotti, "Generation of multiphoton entangled quantum states by means of integrated frequency combs," Science **351**, 1176–1180 (2016).
18. M. Kues, C. Reimer, P. Roztocki, L. R. Cortés, S. Sciara, B. Wetzel, Y. Zhang, A. Cino, S. T. Chu, B. E. Little, D. J. Moss, L. Caspani, J. Azaña, and R. Morandotti, "On-chip generation of high-dimensional entangled quantum states and their coherent control," Nature **546**, 622–626 (2017).
19. M. Afzelius, C. Simon, H. de Riedmatten, and N. Gisin, "Multimode quantum memory based on atomic frequency combs," Phys. Rev. A **79**, 052329 (2009).
20. M. Afzelius, I. Usmani, A. Amari, B. Lauritzen, A. Walther, C. Simon, N. Sangouard, J. Minář, H. De Riedmatten, N. Gisin, and S. Kröll, "Demonstration of atomic frequency comb memory for light with spin-wave storage," Phys. Rev. Lett. **104**, 040503 (2010).
21. Z. Zheng, O. Mishina, N. Treps, and C. Fabre, "Atomic quantum memory for multimode frequency combs," Phys. Rev. A **91**, 031802 (2015).
22. D. Aumiler, "Coherent population trapping in 87rb atoms induced by the optical frequency comb excitation," Phys. Rev. A **82**, 055402 (2010).
23. A. A. Soares and L. E. E. de Araujo, "Coherent accumulation of excitation in the electromagnetically induced transparency of an ultrashort pulse train," Phys. Rev. A **76**, 043818 (2007).
24. V. A. Sautenkov, Y. V. Rostovtsev, C. Y. Ye, G. R. Welch, O. Kocharovskaya, and M. O. Scully, "Electromagnetically induced transparency in rubidium vapor prepared by a comb of short optical pulses," Phys. Rev. A **71**, 063804 (2005).
25. A. Zhang, V. A. Sautenkov, Y. V. Rostovtsev, and G. R. Welch, "Observation of coherent effects using a mode-locked rubidium laser," J. Phys. B **50**, 035503 (2017).
26. D. A. Long, A. J. Fleisher, D. F. Plusquellic, and J. T. Hodges, "Electromagnetically induced transparency in vacuum and buffer gas potassium cells probed via electro-optic frequency combs," Opt. Lett. **42**, 4430–4433 (2017).
27. D. Budker, W. Gawlik, D. F. Kimball, S. M. Rochester, V. V. Yashchuk, and A. Weis, "Resonant nonlinear magneto-optical effects in atoms," Rev. Mod. Phys. **74**, 1153–1201 (2002).
28. N. Šantić, D. Buhin, D. Kovačić, I. Krešić, D. Aumiler, and T. Ban, "Cooling of atoms using an optical frequency comb," Sci. Rep. **9**, 2510 (2019).
29. S. Hopkins, E. Usadi, H. Chen, and A. Durrant, "Electromagnetically induced transparency of laser-cooled rubidium atoms in three-level λ-type systems," Opt. Commun. **138**, 185–192 (1997).
30. D. Felinto, C. A. C. Bosco, L. H. Acioli, and S. S. Vianna, "Coherent accumulation in two-level atoms excited by a train of ultrashort pulses," Opt. Commun. **215**, 69–73 (2003).
31. T. Ban, D. Aumiler, H. Skenderović, and G. Pichler, "Mapping of the optical frequency comb to the atom-velocity comb," Phys. Rev. A **73**, 043407 (2006).
32. D. A. Steck, "Rubidium 87 D line data," 2001, http://steck.us/alkalidata.
33. Y. Niu and S. Gong, "Enhancing Kerr nonlinearity via spontaneously generated coherence," Phys. Rev. A **73**, 053811 (2006).
34. D. Hayes, D. N. Matsukevich, P. Maunz, D. Hucul, Q. Quraishi, S. Olmschenk, W. Campbell, J. Mizrahi, C. Senko, and C. Monroe, "Entanglement of atomic qubits using an optical frequency comb," Phys. Rev. Lett. **104**, 140501 (2010).
35. H. J. Metcalf and P. V. D. Straten, *Laser Cooling and Trapping* (Springer, 1999).
36. E. Ilinova, M. Ahmad, and A. Derevianko, "Doppler cooling with coherent trains of laser pulses and a tunable velocity comb," Phys. Rev. A **84**, 033421 (2011).
37. D. J. Fulton, R. R. Moseley, S. Shepherd, B. D. Sinclair, and M. H. Dunn, "Effects of Zeeman splitting of electromagnetically-induced transparency," Opt. Commun. **116**, 231–239 (1995).